Title

Ultrafast time resolved x-ray diffraction, extended x-ray absorption fine structure and x-ray absorption near edge structure

Journal

Journal of Applied Physics, 112(3)

ISSN

0021-8979

Authors

Er, Ali Oguz
Chen, Jie
Rentzepis, Peter M

Publication Date

2012-08-01

DOI

10.1063/1.4738372

APPLIED PHYSICS REVIEWS—FOCUSED REVIEW

Ultrafast time resolved x-ray diffraction, extended x-ray absorption fine structure and x-ray absorption near edge structure

Ali Oguz Er,[1] Jie Chen,[2] and Peter M. Rentzepis[1,a)]
[1]*Department of Chemistry, University of California, Irvine, California 92697, USA*
[2]*Key Laboratory for Laser Plasmas (Ministry of Education) and Department of Physics, Shanghai Jiao Tong University, Shanghai 200240, China*

(Received 23 February 2012; accepted 14 May 2012; published online 2 August 2012)

Ultrafast time resolved x-ray absorption and x-ray diffraction have made it possible to measure, in real time, transient phenomena structures and processes induced by optical femtosecond pulses. To illustrate the power of these experimental methods, we present several representative examples from the literature. (I) Time resolved measurements of photon/electron coupling, electron/phonon interaction, pressure wave formation, melting and recrystallization by means of time resolved x-ray diffraction. (II) Ultrafast x-ray absorption, EXAFS, for the direct measurement of the structures and their kinetics, evolved during electron transfer within molecules in liquid phase. (III) XANES experiments that measure directly pathway for the population of high spin states and the study of the operating mechanism of dye activated TiO_2 solar cell devices. The construction and use of novel polycapillary x-ray lenses that focus and collimate hard x-rays efficiently are described.
 [http://dx.doi.org/10.1063/1.4738372]

TABLE OF CONTENTS

I. INTRODUCTION

The development of ultrafast lasers has brought new capabilities in time resolved studies not only in optical spectroscopy, but also in other areas of science such as x-ray and electron beam spectroscopy. Powerful femtosecond (fs) laser pulses generated by tabletop laser systems are employed to produce femtosecond electron and x-ray pulses[1–4] in the form of characteristics emission lines as well as x-ray continua in the keV range, that have been used to detect and measure directly transient structures with sub-Angstrom and subpicosecond resolution. One important advantage of the laser driven x-ray systems is the precise synchronization of the pump optical pulses with the probe x-ray or electron beam pulses. Thus, the basic ultrafast pump and probe experimental technique that was utilized for ultrafast time resolved optical studies[5] is now implemented in the hard x-ray region. In the time resolved transient structure experiments presented in this article, an optical pump pulse, is used to excite the sample and an accurately synchronized X-ray probe pulse monitor the formation and decay of transient species, their structure, and dynamics. XANES, X-ray near edge structure, EXAFS, X-ray absorption fine structure, and X-ray diffraction are the most commonly used time resolved X-ray methods.

The number of time resolved X-ray absorption studies published so far is quite limited compared to the number of optical studies. The time resolved X-ray studies include gas phase ultrafast X-ray absorption experiments[6] of gaseous SF_6 and time resolved X-ray absorption spectroscopy (XAS) experiments, with 14 ns resolution that describe the transient molecular structure in the liquid phase.[7,8] The chemical shift of photo-excited aqueous [Ru(bpy)3] was also measured with ~100 ps resolution[9] and later a similar tabletop x-ray system was utilized to determine the structure of photo-excited Fe(CN) in water with 30 ps resolution.[10] The XANES associated with the photoinduced Fe(II) spin crossover reaction has been investigated by means of 70 ps, 7.1 keV, tunable X-ray pulses derived from the advanced light source.[11]

a)E-mail address: pmrentze@uci.edu.

Ultrafast time-resolved EXAFS imaging techniques have been employed to study the dynamics of the femtosecond laser ablation of aluminum in an energy range well above the ablation threshold. They have shown that photomechanical fragmentation and vaporization were the dominant mechanisms for the production of liquid nanoparticles and neutral atoms.[12] Time-resolved X-ray liquidography has also been applied to study structural dynamics and spatiotemporal kinetics of many molecular systems including diatomic molecules, haloalkanes, organometallic complexes, and protein molecules over timescales from picoseconds to milliseconds.[13] Furthermore, time-resolved x-ray diffraction and optical studies investigations of out-of-equilibrium switching dynamics of a molecular Fe(III) spin-crossover solid have has determined the dynamics initiated by subpicosecond local photoswitching, volume expansion, and thermal switching processes.[14] Recently, the local structure of the copper phase of a $CuO–CeO_2/Al_2O_3$ catalyst and its activity on the total oxidation of propane has been studied using time-resolved XAS in the transmission mode coupled with on-line mass spectrometry.[15] A recent femtosecond time resolved XANES study showed that after fs excitation of the singlet metal-to-ligand-charge-transfer band (MLCT), the lowest quintet state of aqueous iron(II) tris(bipyridine) was formed.[16]

Electron transfer in iron and cobalt liquid complexes, in solution, has also been studied using time resolved EXAFS with subpicosecond and sub-Angstrom resolution.[17,18] These studies determined that the mechanism of the electron transfer processes, initiated by photo-excitation in the charge transfer band, can be either intra or intermolecular depending on the structure of the molecule and degree of freedom of rotation of the ligand. In addition, several electron and x-ray ultrafast time resolved experiments have reported on the transient changes in the lattice structure of single crystals after excitation with an fs optical pulse.[3,19–31]

In this paper, we present the experimental data for three different processes that illustrate how these methods make it possible to determine, in real time, transient structures and very short lifetimes phenomena that in conjunction with density functional theory (DFT) calculation determine the operating mechanism of many basic processes and reactions. The experiments described were performed by using a tabletop laser system that generated femtosecond optical pump pulses and subpicosecond hard 6-22 keV x-ray probe pulses.

Of the vast number of topics that can be investigated with these techniques, we will restrict this review to x-ray diffraction, extended x-ray absorption fine spectroscopy (EXAFS) and X-ray near edge structure (XANES) time resolved studies aimed at illustrating the versatility of these techniques and capability for direct detection and measurement of transient structures and the dynamics of transient excited states and intermediate species evolved during the cause of processes induced by fs optical pulses.

Ultrafast time-resolved x-ray diffraction experiments have been performed with nanosecond and picosecond resolution,[32] and lately, it has become possible to measure the structure of transients with subpicoseconds and sub-Angstrom resolution. These experiments provide the means for measuring directly ultrafast transient phenomena, induced on a solid by femtosecond optical or other type of pulses. Intermediate(s) and short-lived phenomena that have been identified and measured by these techniques, include, photon/electron interaction, electron thermalization, electron/phonon coupling, and pressure waves and phase transition and atomic order/disorder processes such as melting and recrystallization.

The diffraction of monochromatic x-ray radiation from a crystal is governed by Bragg's law, which suggests that a very small change in the crystal interatomic spacing will result in a measurable shift in the diffracted angle. The relation between the angle shift Δq and the lattice spacing d is given by differentiation of Bragg's equation,

$$\Delta d/d = -\Delta q/\tan q.$$

The angle shift, therefore, is represented by the change in the spacing of the diffracting planes of the crystal. When laser radiation is absorbed by a thin surface layer of a crystal, the temperature distribution and the associated stress in the bulk of the crystal will become nonuniform causing the lattice spacing to distort. Such nonuniform lattice spacing distribution inside the crystal causes the diffraction signal to be scattered over a range of angles corresponding to the changes in lattice spacing. If the divergence of the monitor x-ray beam is sufficiently large to cover all of these angles, then the recorded signal will contain all of the information regarding lattice space changes. Experimentally, the entire rocking curves, both signal and reference, have been recorded simultaneously on a large area x-ray CCD detector, in one shot, using a divergent, 0.6 ps x-ray pulsed beam. The recorded x-ray signal is essentially the convolution of the crystal response to the probing x-ray pulse and the time resolution depends not only on the duration of the pump and probe pulses and material response, but also on the propagation time of the fs pulses inside the sample and x-ray lenses.

X-ray diffraction is probably the best known means for the study of the structure of solids on the atomic level; however, its application to liquid phase is rather limited because of the absence of order in the sample. Many elementary reactions in chemistry and biology, however, occur in the liquid phase. Therefore, there is need for efficient and accurate methods that make it possible to study the structure of the ultrafast transient states and species evolved in course of reactions in the liquid state. It is widely accepted that for the determination of structures in the liquid phase x-ray absorption techniques[33,34] such as XANES and EXAFS may be advantageously employed, because they can inherently measure rather easily and very accurately the local structure of molecules, such as bond length changes, charge distribution, oxidation-reduction, and coordination number of atoms and molecules. X-ray absorption has also the advantage of being very sensitive only to the particular atom that absorbs the x-ray radiation that consequently determines the structure of the first few coordination layers adjacent to the absorbing atom and is not affected by solvent or impurities as long as they do not contain the absorbing atom. Many fundamental processes in nature, such as electron and protons transfer reactions and phase transitions involve dynamic changes in their atomic arrangements that may take place on time-scales

comparable to the oscillation periods of atoms and molecules. Therefore, to measure and understand the dynamics of chemical and biological process on such ultrafast time-scales, structural information with picosecond and femtosecond time resolution is necessary. Expanding EXAFS to the ps and fs time domain has been rather important and quite challenging, because in EXAFS, the processes of electron ejection, backscattering and interference are extremely fast. For inner shell electrons with KeV energies, these processes are essentially completed within a few femtoseconds. To display these data XANES and EXAFS should be able to take a real time; instantaneous picture, of the atoms involved in an interaction[6,35] and display their transient bond distance and local structure as a function of time (fs) immediately after excitation. Owing to improved techniques that generate ultrashort optical and hard x-ray pulses, fs time resolved x-ray absorption experiments may be performed at many university laboratory because the required ultrafast characteristic lines for diffraction and broadband x-ray continua used as probe pulses in x-ray absorption can now be generated by tabletop laser-induced plasma x-ray systems.

II. EXPERIMENTAL SYSTEM

The experiments described in this paper were performed on a tabletop Ti:Sapphire fs, laser system that generates both the optical fs pump and keV x-ray characteristics lines and continuum subpicosecond probe pulses. It consists of a laser oscillator that emits 80 fs pulses at 82 MHz, that seed a regenerative amplifier followed by a multi-pass power amplifier, which generates 100 fs, 100 mJ, 800 nm, 10 Hz pulses that are focused onto a 0.5 mm, or 0.25 mm diameter moving Cu, Mo, or W wire located inside a vacuum chamber, Fig. 1(a), thus, producing an electron plasma which mediated the generation of hard x-rays. The laser plasma generated x-ray radiation exits the chamber through a 0.25 mm thick Be window, covered by rolling plastic tape that protects it from metal debris emitted by the evaporated metal. The time width of the x-ray pulse were measured by the thin crystal technique and found to be 0.6 ps. The x-ray spectra emitted by the W, Cu, and Mo wires which consist of both characteristic lines and continua were measured using an x-ray detector (2D CCD) and multichannel analyzer. The x-ray energy range used in our experiments was between 6 KeV and 22 KeV, with the low limit determined by the transmission of the chamber window, the plastic tape, air and the high energy limit set by the detector sensitivity and polycapillary lens, transmission, Fig. 1(b). The spectra shown in Fig. 2 consist of both continuum radiation suitable for ultrafast x-ray absorption spectroscopy studies and characteristic emission line suitable for x-ray diffraction measurements. The x-ray spectra recorded display the raw count rate data without correction for x-ray chamber windows loss, air transmission, and detector efficiency. We have estimated that for a 20 mJ laser pulse energy impinging on a copper wire target, 46% of the x-ray photons transmitted through the x-ray chamber belong to the CuK_α characteristic line. The Si(111) energy-dispersive crystal employed allows for the entire x-ray absorption spectrum to be recorded simultaneously. This is important, if not mandatory, for measurements that utilize x-rays generated by high intensity fs laser pulses because the shot to shot fluctuations of the x-ray flux can be high and affect adversely the entire spectrum.

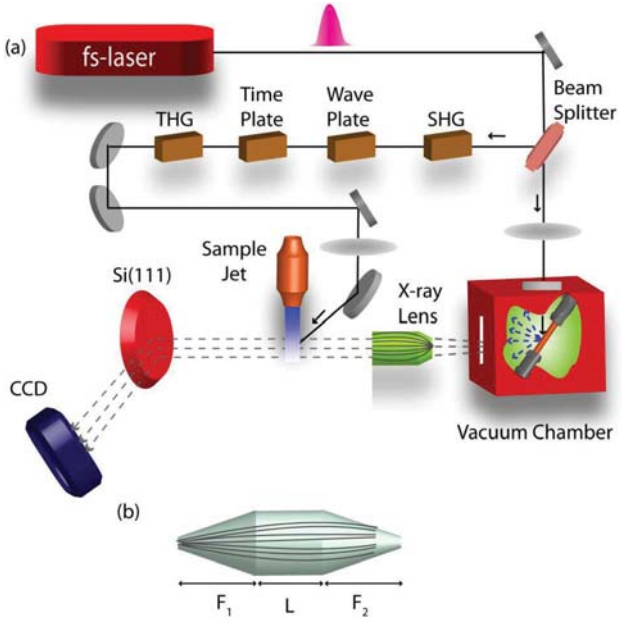

FIG. 1. Experimental systems: (a) fs laser and x-ray pulse generating systems showing the collimating polycapillary lens, dispersive spectrometer, detector, and sample. (b) Focusing polycapillary lens.

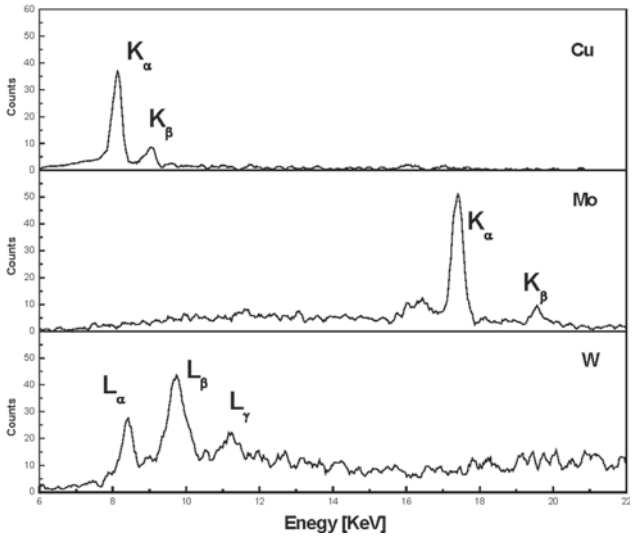

FIG. 2. X-ray spectra emitted by Cu, Mo, and W wire.

In the past couple of decades, table-top systems have utilized fs laser pulses to generate fs hard x-rays pulses by interaction with metals.[6,32,34] However, although the x-ray flux generated by the table systems is large at the source, the x-rays flux that impinges on the sample, located several centimeters away from the source, contains only a very small fraction of the total amount of the generated x-rays owing to the 4π x-ray spread. This weak x-ray flux at the sample restricts the practical use of table top x-ray sources to only few experiments that have high absorption cross section and do not require exposure time to obtain the necessary data. Therefore, optics that increase the x-ray flux on the sample

are needed to improve the signal to noise ratio and decrease the experimental exposure time. Curved reflection optics increase the x-ray flux by a very small factor, in contrast polycapillary x-ray focusing optics[36] focus the x-rays tightly and thus increase the x-ray flux on the sample by factor of 1000 or more.[37] Comparison of various focusing x-ray optics and their employment for femtosecond x-ray diffraction and absorption has shown that polycapillary lenses concentrate the largest number of photons onto a small spot.[38]

A. Polycapillary x-ray lenses

Conventional x-ray optics have been used in basic science, technology, and medicine for many years and lately polycapillary lenses have started to be employed in a few fields of science. We have used polycapillary lenses, for several years, to focus hard x-rays onto a small spot on the sample, thus increase the x-ray flux by a factor of ~3000 and perform experiments that w could not be performed previously without the polycapillary lenses.

The polycapillary x-ray lenses are composed of several million hollow capillaries (with IDs between 2 and 15 μm) bundled together to form a single monolithic structure and gently bend to achieve the curvature[36] required for the x-rays to enter at an angle smaller than the total reflection critical angle, traverse through the hollow quartz tubes via total external reflection on the inner surface of the x-ray capillary channels with a simple roughness correction and then be focused onto a few μm area of the sample, Fig. 1. The largest advantage of the x-ray lenses is to reduce the inverse-square dependence of x-ray intensity versus distance from the source by collecting and focusing or collimating the x-rays, thus increasing the gain in x-ray flux at the sample by orders of magnitude. A typical focusing lens is shown in Fig. 1(b). Collimating monolithic x-ray half-lens lenses are used to capture the diverging x-rays emitted by the x-ray source and collimate them to a parallel x-ray beam suitable for x-ray diffraction, in Fig. 1(a). Focusing polycapillary lenses are bent to curvature R.

$$R > 2d/\theta_c^2,$$

where d is the diameter of the channel, R the radius of curvature and □c the critical angle of total reflection, which is linearly proportional to the x-ray wavelength. The inequality suggests that x-rays will not be transmitted when the geometry of the channel does not satisfy this inequality.[39] For monolithic x-ray lenses, the transmission efficiency depends on the photon energy and geometric parameters of the channels (diameter and length), its shape and size. x-rays that have grazing angles larger than the critical angle of total reflection for a given material are eliminated; this means that while both continuum and characteristic Cu lines are transmitted through the polycapillary x-ray lens x-rays at energies above 30 and below 3 keV are eliminated and therefore the lens effectively functions as a bandpass filters.

The focal spot size is defined as the minimum full width at half maximum (FWHM) of the space distribution of the measured power density. The gain in power density obtained by the lens is the ratio of the x-ray intensities at the focal spot of the lens with and without the lens. For an isotropic x-ray source, the gain (K) is

$$K(E) = \left(\frac{L}{f_1}\right)^2 \frac{S_{in}}{S_{spot}}\ \eta(E),$$

where η is the transmission efficiency of the lens for x-rays of energy E, L the distance from the x-ray source to the focal spot of lens, S_{in} the entrance area of the lens, S_{spot} the area of the focal spot and f_1 the input focal distance. The gain of the lens is directly related to the amplification of the x-ray beam power density by the lens. Another useful experimental parameter is the equivalent distance (L_{eq}).

$$L_{eq} = L/K^{1/2},$$

where L_{eq} is the distance between the x-ray source and the point where the power density of x-rays emitted by the x-ray source is equal to the power density at the focus spot. An equivalent distance of 2–3 mm was achieved with our x-ray lens. This means that we performed experiments equivalent to having the sample at a point 2–3 mm away from the x-ray source rather than the actual 124 mm distance from it.

Although the monolithic lens has the advantage of collecting x-rays from a large solid angle, the focal spot size cannot be as small as that can be obtained by single capillary. To achieve such a small x-ray focus spot, one may construct a monolithic lens tapered to a single capillary that may be used to study single molecule x-ray structures.

For ultrafast time resolved studies, pulse broadening is an important parameter, which is associated with (a) the propagation of the x-ray pulse inside an individual capillary and with the varying length of the capillaries, see Fig. 1(b). The broadening of the x-ray pulse was measured to be less than 50 fs after it propagated through a 5 μm diam. Capillary was broadened by 0.6 ps after traveling through the different length capillaries of our 51.5 mm lens. Because broadening of the pulse was only 0.6 ps, these lenses were deemed suitable for use in ultrafast, subpicosecond, time-resolved x-ray diffraction, and absorption experiments. A few of the first applications of polycapillary x-ray lenses for time resolved diffraction and absorption experiments are described in the following sections of this article.

B. Ultrafast resolved optical x-ray system

The polycapillary x-ray lens that we used in the experiments presented here has a length of L = 51.5 mm and focal lengths of F1 = 55.0 mm and F2 = 16.7 mm. Synchronization of the x-ray and optical pulses was achieved by guiding the fundamental 800 nm pulse through the same path that the x-ray travels and intersecting it with the 266.7 nm pump pulse inside a thin potassium dihydrogen phosphate (KDP) crystal, which is cut at the third harmonic generation (THG) phase matching angle. A dielectric mirror, placed where the sample will be during the course of the x-ray experiments, is used to direct the 800 nm and 266.7 nm pulses onto each other, overlap, and effectively interact inside the KDP crystal generating the 400 nm pulse. The 800 nm and 266.7 nm

beams were filtered out by a BG39 bandpass filter that transmits only the 400 nm difference pulse. By measuring the intensity of the 400 nm beam generated by the interaction of the 266.7 nm and 800 nm beams as a function of the distance between them, the overlap time of the optical pump and x-ray probe pulse was accurately established to within less than 1 ps. The time and space synchronization of the optical and x-ray pulses was then achieved and confirmed by monitoring the x-ray diffraction from a thin Si(100) crystal. Owing to the divergence of several degrees and the tight focusing of the x-rays by the x-ray lens, we were able to conduct the ultrafast x-ray absorption experiments that previously were very time consuming and difficult to perform without the x-ray lenses.

III. TIME RESOLVED X-RAY DIFFRACTION

To estimate the upper limit of the x-ray pulse width we have adopted the thin crystal technique,[6,40,41] where the cross correlation between the x-ray and optical pulses were measured by monitoring the x-ray diffraction from a thin 520 nm thick Si (100) crystal grown on a sapphire substrate. The Bragg x-ray reflection from Si (100) is easily distinguished from the sapphire substrate reflection because of the difference in their lattice constants (measured angle about 0.6°). In a standard pump/probe setup the Si crystal is illuminated with the second harmonic, 400 nm, at a fluence of 10–20 mJ/cm^2 and probed by the Cu Kα x-ray pulse. The absorption depth of the second harmonic in Si crystal is 100 nm; however, the penetration depth of Cu Kα radiation is more than 25 μm. This difference in penetration depth necessitates the use of a thin crystal in order to match the absorption depths of the optical pump and x-ray probed pulses. The intense femtosecond optical excitation induces a solid-to-liquid phase transition, melting, that leads to a fast drop in the x-ray diffraction signal intensity, within a few hundred femtoseconds, after the pump pulse strikes the Si(100) surface. This is followed by a further gradual decrease in the diffracted signal. This step like response in the x-ray diffraction signal was used to estimate the upper limit of the x-ray pulse duration.[40,41] Figure 3 shows the measured change in the diffraction signal for Si (400) reflection as a function of delay time between the second harmonic

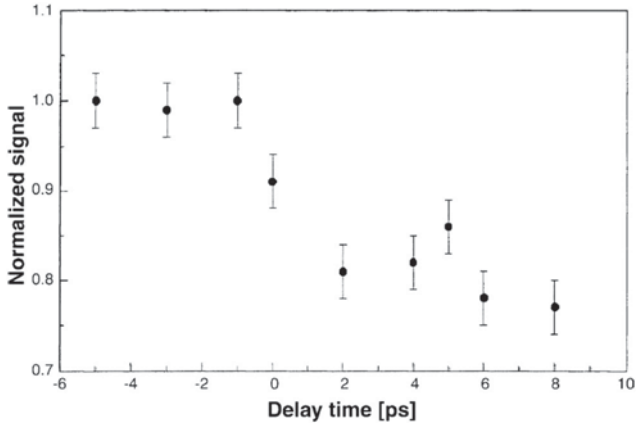

FIG. 3. X-ray intensity as a function of the delay time between the pump optical pulse and the probe x-ray pulse.

excitation and the x-ray probe pulses. We observed a decrease of about 20% in the diffraction efficiency within 2 ps and have also measured the x-ray pulse duration, on the same experimental system when the X-ray lens was removed and replaced with a 300 μm slit, and found that the transit time was similar.

Therefore, the information derived from the Si(100) crystal melting transition time of ~0.6 ps indicates that (a) the upper limit of the x-ray pulse length is less than 0.6 ps; (b) the melting transition process observed for silicon and several other semiconductors[42] is dominated by a nonthermal process initiated by the photon-electron interaction, which is less than 0.6 ps; (c) the pulse broadening attributed to the x-ray polycapillary lens is less than 0.6 ps; (d) the entire ultrafast x-ray system is capable of 0.6 ps.

Experiments performed on thin Au(111) single crystals allowed us to detect and measured directly the basic phenomena and processes that occur after the interaction of ultrashort optical pulses with the surface of a Au(111) crystal.

In the studies presented here, 150 nm Au (111) single crystals were irradiated with 10 Hz, 100 fs, 400 nm pulses and a fluence of less than 15 mJ/cm^2. The transient lattice change that we observed and measured by time resolved x-ray diffraction is a convolution of the strain generated by three processes: The blast wave, the sonic wave, and thermal diffusion. The fraction of Fermi electrons generated with the photon energies used is very small. Photon/electron interaction occurs within the pulse width time, then; electron/phonon coupling was observed, followed by phonon lattice interaction that resulted in the generation of two pressure waves, a blast wave, formed within the excitation pulse width and the well known pressure sonic wave that propagates through the crystal inducing a periodic rocking broadening curve. The lattice near the surface is first compressed by the blast force wave, then expansion is launched owing to the larger amplitude acoustic wave.[24] The periods of the coherent lattice vibration for 150 nm Au(111) are estimated to be 98 ps, which is slightly shorter than the period measured experimentally, owing to the damping of the coherent acoustic oscillations.

When the pump pulse is absorbed by the surface layer of the sample, that has a thickness on the order of the absorption length, a transient elastic stress is formed which generates a pressure wave that propagates through the sample introducing in its path a transient modulation of the lattice parameters.[43–45] For thin films with thickness comparable to the optical absorption depth, a near homogeneous hot electron plasma is generated after the absorption of a femtosecond optical pulse which places the lattice at a stressed state, within a time that is shorter than the lattice response time. Under these conditions, coherent lattice vibrations can be generated[46–48] and in fact have been experimentally observed recently by electron diffraction in thin Al films.[47,49] In films thicker than the light penetration depth, the electron gas temperature generated by femtosecond optical pulse is nonuniform and has been predicted[50] that before electron–electron thermal equilibrium is established, the hot electron gas will interact with the surface to generate a "blast" force that exerts a "pressure" on the lattice in addition to the

thermomechanical load caused by the temperature gradient established across the thickness of the heated region. The magnitude of the hot electron blast force is proportional to the gradient of the electron temperature squared.[51,52] The shock wave generated by the blast force, added to the thermal load resulting from the nonuniform lattice temperature at later times can be very strong and cause changes in both the microstructural and mechanical properties of the material even at lattice temperatures far below the melting point. Our experiments cannot detect the exact time origin of the blast force, which is predicted to be within the pulse width; however, the existence and effect of the blast force were detected and monitored during the measurement of the rocking curve broadening, shown in Fig. 4.[53] It is to be noted though that the blast wave is generated during the very early stages of heating, while the sonic wave achieves its maximum tens of picoseconds later. It is estimated that when a 100 nm gold film is heated by a 100 fs optical pulse the blast force will last ~1.6 ps.[18,54–57] Although the blast force lasts a very short time, 1-2 ps, the expansion wave generated by this force propagates through the crystal for several picoseconds and changes the lattice structure sufficiently to be detected by our time resolved x-ray diffraction experimental system. In contrast, the generation of the sound wave is slower, requires 10-20 ps to develop, and therefore, it is separated enough from the blast wave to be detected at even longer delay times. The blast wave is considered to be a compressive wave that acts on the crystal before the acoustic wave,[24] then lattice expansion is observed due to the launch of the larger amplitude acoustic wave. The influence of the blast wave is relatively small compared to the acoustic wave, consequently it may be masked and appear as the onset of the expansion. The modulation peak shown in the rocking curve of Fig. 4 is assigned to the blast wave, while the broadening of the rocking curve is a result of the strain generated by both the blast and sonic waves. The ultrashort blast force that was formed just at the end of the pumping optical pulse, that in agreement with theoretical calculations,[51,52,58] combines with the wave built by sonic processes to produce the strain distribution detected by our time resolved x-ray diffraction experiment.

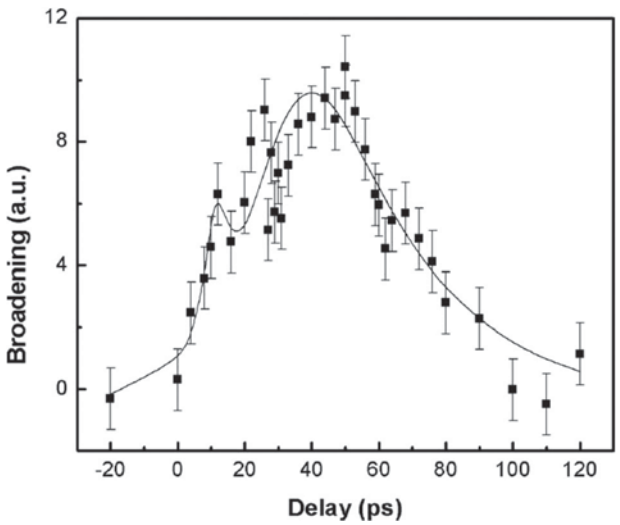

FIG. 4. Broadening of the rocking curve, (FWHM), plotted as a function of time delay. Solid line is calculated fit to experimental data.

Coherent phonons may also be excited and induce lattice vibrations[46] during the propagation of the acoustic and blast waves, and subsequently lattice expansion and contraction. The lattice vibrations generated by the propagation of the acoustic wave have been experimentally observed recently by electron diffraction in 20-nm-thin Al film (8 nm optical length);[47] Tentative theoretical studies based on the two-temperature model (TTM) and the Fermi-Pasta-Ulam anharmonic chain model have been used to explain the experimental coherent lattice vibrations.[59,60] Damping of coherent acoustic oscillations, in a femtosecond laser-heated 400-nm crystalline germanium film with optical length of 200 nm, has been measured by time-resolved XRD.[61] In two cases studied, it was found that when the sample thickness was comparable to the optical absorption depth, the overall effect of the acoustic wave was the expansion of the lattice. In a recent report,[62] the oscillation of the lattice changes were applied to disentangle electronic and thermal pressure contributions to femtosecond laser induced lattice expansion in 90-nm gold single-crystals.

At high excitation fluence, melting of the gold crystal occurred near or above its melting point of 1337.33 K, which was detected by the sudden drop in the x-ray diffraction intensity recorded as a function of time.

To study the atomic structure changes during melting process with high resolution, gradually the optical laser pulse intensity was increased until melting of the crystal surface was detected by sudden changes in XRD intensity while the excitation energy and intensity were kept below the damage threshold. At times before excitation, i.e., 40 ps, the XRD signal was, in all aspects, the same as the one observed at room temperature. As the time delay was increased to a few picoseconds after excitation and the energy of the laser pulse energy became sufficiently high to melt, but not damage, the crystal, a sharp decrease in the total XRD intensity was observed within ~5 ps after irradiation of the 150-nm Au(111) crystal. It was followed by an increase in the diffraction intensity after approximately 10 ps, which continued to increase for 40 ps after excitation, and recovered to its original diffraction intensity at about 100 ps after excitation, Fig. 5. The diffraction recorded after the crystal was cooled was the same as the one before excitation, which suggests that the gold crystal remains intact and without damage throughout the experiment. The entire process attributed to melting and annealing of the gold crystal, may be considered to consist of three stages: (i) the lattice disorder, phase-transition, melting or lattice structure softening by removal of crystal defects that cause internal stresses inside the crystal; (ii) the grain growth phase—if the lattice temperature is kept under annealing conditions, grain growth will occur and the microstructure will start to coarsen inducing new internal stresses; (iii) the recrystallization phase—the new strain-free grains nucleate and grow to replace those deformed by internal stresses.

The sharp decrease in XRD intensity is attributed to melting or premelting of the Au(111) crystal. Because the pumping energy is limited, the ultrafast melting/premelting

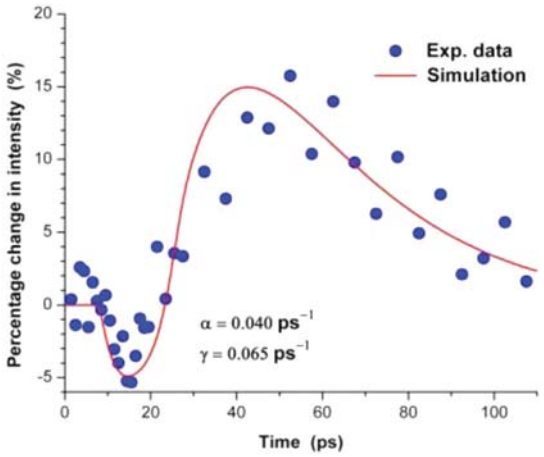

FIG. 5. Change in x-ray diffraction intensity as a function of time. Steep decrease in intensity designates melting. Dots experimental, line simulation. Reproduced with permission from J. Chen, W.-K. Chen, J. Tang, P. M. Rentzepis, PNAS **108**, 18887–18892 (2011). Copyright © 2011.

process occurs only in the area within the optical path absorption depth (16.9 nm), while the x-ray pulse penetrates and probes the entire 150-nm-thick gold crystal. Consequently, only a small fraction (ca. 11%) of the x-ray intensity is expected to be affected by surface melting. The experimental data show, Fig. 5, a decrease in the diffraction intensity of 6%–8%. The rate of the melting process was estimated, from the experimental data, to be $3 \times 10^{11}\,s^{-1}$, which is in agreement with the previously reported values for thermal melting.[63] Based on phonon/phonon and phonon/lattice interaction rates, which are in the $10^{11}\,s^{-1}$ rate, and the time-resolved XRD data, the observed process was assigned to thermal melting, rather than electronic melting. The increase in the XRD intensity from 92%–94%, starting at approximately 7 ps to ~116% after 40 ps was attributed to recrystallization, mosaic crystal formation, and softening of the inner part of the crystal. For phonon $t_G = \sim 5$ ps in graphite and graphene,[64] and for silicon $2\Gamma = 0.48\,cm^{-1}$, where $\Gamma = 1/\tau$ (Ref. 65); homogeneous melting in epitaxial Ag(001) films occur within the first few picoseconds after excitation with a femtosecond laser pulse.[66] It has been reported that after approximately 10 ps the surface heat energy and acoustic wave cause the lattice temperature in the crystal to increase through phonon/phonon interaction. However, the optical excitation pulse energy that was used is neither enough to penetrate throughout the crystal, nor sufficient to melt the entire crystal. Therefore, only a softening of the interatomic potential of the inner areas of the crystal is expected.[67] Generally speaking, materials become softer after optical heating and if the lattice temperature is close to the melting point, and is maintained at that level for a period of time, the lattice will anneal, recrystallize, and form a mosaic crystal structure due to strain-free crystallization. The mosaic crystal may give higher XRD intensity than the original single-crystal structure when measured with an x-ray beam that is not perfectly collimated and has also a certain wavelength distribution. In fact, data presented in Fig. 5 show higher diffraction intensity for a period of time when the crystal is cooling after the melting phase disorder lattice.

Time resolved x-ray diffraction has been used frequently to study the detail mechanism of protein structural transition by means of synchrotron ~100 ps x-ray pulses,[68,69] which may be considered their major limitation for time resolved x-ray diffraction experiments. The development of x-ray free electron lasers (XFELs) will overcome this restriction and are expected to generate much shorter x-ray pulses, data collection rate, and structural resolution.[70] Peak brilliance of XFEL sources are 10^9 times higher than conventional synchrotron sources, pulse duration is ~10 fs, and in addition XFEL sources have a high degree of transverse coherence. With the current 3rd generation of synchrotrons, it is possible to study the structures of short-lived species and their formation and decay kinetics. However, it is not possible to substantially lower the emittance of a storage ring below the values achieved in this third generation machines. Therefore, Femtosecond time resolved XFEL opens up a new window to determine the coherent wave packet motions and potential energy surfaces. The European XFEL which is to become fully functional sometime in 2015 should is also expected to generate extremely intense x-ray pulses for time resolved x-ray diffraction experiments. The Linac coherent light source (LCLS) has shown the possibility for the interaction of single atoms, with intense x-ray pulses[71] and the creation and diagnosis of solid density plasma,[72] and implementation of x-ray laser driven by rapid K-shell photoionization using pulses from XFEL.[73] Diffraction intensities of lysozyme nanocrystals using 2 keV photons to determine the structure by molecular replacement[74] have been already investigated.

Time resolved x-ray liquidography (TRXL) has emerged as another important tool for the study of transient molecular structures owing to the fact that the scattering signal is very sensitive the chemical species which have characteristic diffraction signals.[13,75] In this method, short x-ray pulses of 100-150 ps duration emitted by the synchrotron and ultrashort pulses generated by femtosecond lasers are combined to obtain direct structural information that is difficult to extract using ultrafast optical spectroscopy alone.[76] In some TRXL experiments, instead of monochromatic x-ray pulses, polychromatic pulses are used to increase the signal-to-noise ratio. Time resolved x-ray liquidography has been successfully employed to investigate several transient phenomena, including: the photodissocication of $HgBr_2$ (Ref. 77) determine the excited state structure of the organometallic compound PtPOP,[78] the structural dynamics of the iodine elimination reaction of 1,2-diiodoethane ($C_2H_4I_2$) in cyclohexane,[79] light induced effects on protein-coated gold nanoparticles,[80] and the anisotropic x-ray scattering effects patterns of myoglobin protein molecules.[70]

In this and other time resolved x-ray diffraction experiments, the evolution of the changes in the structure of the crystal has been monitored with sub-Angstrom-space and sub-picosecond time resolution and has mapped the entire cycle of the processes induced by an fs optical pulse.

In the following section, we present a study that describes the formation, decay, and the structure of excited states and fast decaying intermediate species of a molecule in the liquid phase that undergoes electron transfer after excitation by a single fs optical pulse.

IV. TIME RESOLVED EXAFS APPLIED TO ENERGY TRANSFER

Energy transfer by means of electrons,[81,82] protons,[32,83,84] and other forms[85,86] are commonly occurring processes in nature and many areas of science. Among the most common processes, electron transfer has been the subject of numerous theoretical and experimental studies, however, very little information is available concerning the structure of the transient states and intermediate species evolved that drive the mechanism of the energy transfer process. Lately, however, owing to the generation of ultrashort hard x-ray and electron pulses by synchrotron and tabletop laser sources, it is possible to measure directly the transient structures in liquids by means of time resolved x-ray absorption[34,87] and to determine the mechanism responsible for electron transfer in molecules in the liquid phase.

Iron Fe(III)(ox)3 metal complex, where ox = $[C_2O_4^{2-}$ was selected because it is known to transform to Fe(II) after optical excitation,[88] and both the spectra and extinction coefficients are well documented in the literature.[89–91]

A. Electron transfer in metal complexes

Fe(III) and Co(III) complexes have been studied in the liquid phase for several years.[92–95] Yet the formation and decay rates of the excited states and intermediate species have not been reported at least in the fs and ps time regime, even though the quantum yield of the electron transfer has been investigated in depth and is used for actinometry.[96] The mechanism of this process has been studied by both steady state and pulsed irradiation and the data obtained suggest that the quantum yield for the formation of Fe(II) exceeds 1.0 when the sample is excited with 250-400 nm light. To justify such high quantum yield, it is expected that the mechanism of the primary process would involve dissociation of the metal complex and the generation of fragments that react with the parent molecules transferring an electron from the fragment to the metal thus initiating the Fe(III) → Fe(II) process. Based on these data, the most probable ET mechanism that has been proposed[92] is

$$\mathrm{Fe(III)(ox)}_3 \xrightarrow{h\nu} \mathrm{Fe(II)(ox)}_2 + \mathrm{(ox)}^- \quad (1a)$$

$$\mathrm{Fe(II)(ox)}_2 + \mathrm{(ox)}^- \rightarrow \mathrm{Fe(II)(ox)}_3 \quad (1b)$$

$$\mathrm{Fe(III)(ox)}_3 + h\nu \rightarrow \mathrm{Fe(II)(ox)}_3. \quad (2)$$

Several interesting ns to ms time resolved flash photolysis experiments have been reported that provide valuable insight into this processes.[97] Even at the rather slow ns/ms experiments, it is evident that the first order dependence of the Fe(III) complex decomposition to Fe(II) involves a Fe(III)/Fe(II) electron transfer.[97] However, these experiments were of low resolution and could not distinguish between reaction 1 and 2. This ambiguity is very important because it pertains a primary processes, on which the electron transfer mechanism is based upon and is expected to proceed with picosecond rate or faster. Therefore, to determine the ET operating mechanism, we have extended these studies to the optical and x-ray absorption picosecond and femtosecond regime. The metal complex experiments presented in this article were conducted in air at room temperature using 100 fs, 0.3 mJ, 267 nm excitation and broad 600 fs hard x-ray continuum probe pulses.

In addition to the fs/ps experimental system, a 6 ns Nd:YAG laser was used for ns to ms experiments. The pump pulse for the nanosecond experiments was the third harmonic, 355 nm of a Nd:YAG laser, while the 400 nm SHG and 267 nm THG of the Ti:Sapphire served as the pump pulse(s) for fs/ps experiments. The probe beam used with the fs and ps optical experiments consisted of a broad continuum, of the same duration as the pump pulse that covered the 300-600 nm spectral region, while a high pressure xenon lamp provided the probe continuum for ns to ms optical experiments. The detectors were a fast photomultiplier coupled to an oscilloscope and a computer controlled CCD system for nanosecond experiments and ps/fs experiments, respectively. The femtosecond absorption data, Fig. 6, show that an intermediate state was formed at 430 nm, immediately after excitation, that reaches its maximum absorption intensity after 2.6 ps and then remained constant for at least 610 ps. Using the nanosecond system, it was determined that 430 nm band decays with a lifetime of 4 ns and the processes that cause its formation and decay are shown in Eqs. (1a), (1b), and (2) and are also in accord with the mechanism derived from previous time resolved experimental data. Subsequently, the transient structures determined by time resolved EXAFS, presented in a later section of this paper, were correlated with the transient species identified by fs optical spectroscopy and used to derive the Fe(III)/Fe(II) electron transfer mechanism.

B. Solvated electrons

A 500-800 nm transient absorption band with maximum at 720 nm was formed immediately after excitation with 266 and 267 nm pulses, Fig. 7, which is essentially identical to the well known broad, structureless, absorption band of

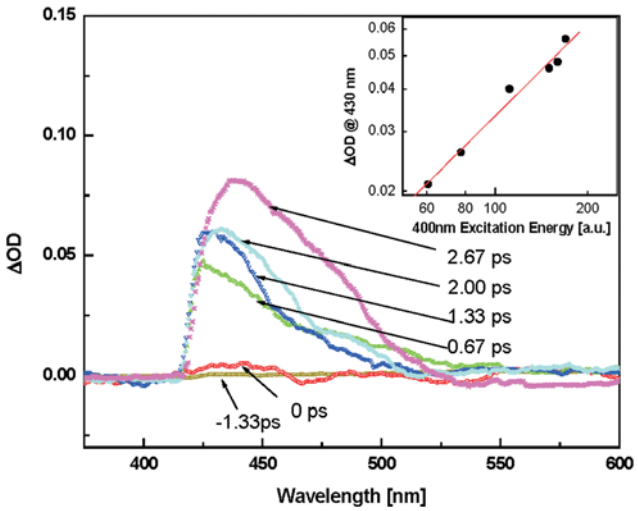

FIG. 6. Femtosecond transient absorption spectra of ferrioxalate in water excited by 400 nm pulses. Insert: Energy dependence of the transient optical density at 430 nm.

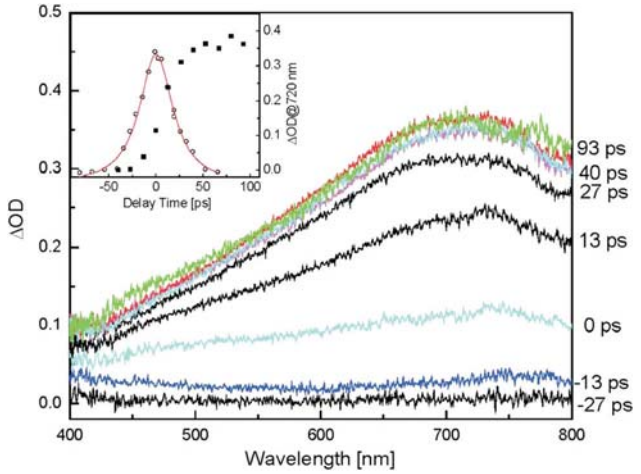

FIG. 7. Picosecond transient absorption spectra of 1.0×10^{-3} M cobaltoxalate in water using 266 nm excitation. Inset: transient kinetics at 720 nm (solid square points) and the 45 ps pulse width (open circle points fitted with solid line).

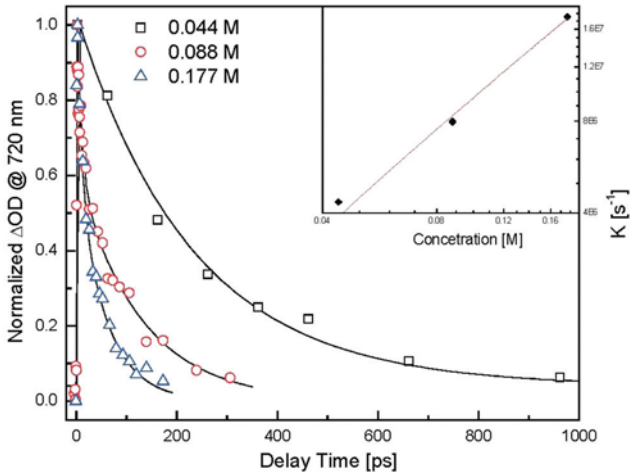

FIG. 9. Time resolved transient kinetics of Ferrioxalate in water at different concentrations after 266/267 nm excitation (square: 0.044 M, circle: 0.088 M and triangle: 0.177 M). The solid lines are exponential decay fits to the experimental data. Inset: the reaction rate constant at different concentration and the solid line is a linear fit to the experimental data.

solvated electrons in water.[98,99] The decay lifetime of this absorption band is shown in Fig. 8 and its dependence on concentration in Fig. 9. The formation and decay kinetics were in agreement with the reported literature values,[98,99] and by comparison with the quantum yield of ferrocyanide, which is ~1,[100,101] the quantum yield for the photodetachment of an electron from this iron complex was estimated to be 0.05.

C. Time resolved EXAFS data

The most relevant data for understanding the mechanism of electron transfer are the one that display accurately the transient structures of the ET process. To record this data, the iron complex was dissolved in water to a concentration of 1 g/ml, which corresponds to $\mu x \sim 1$. The fs optical pump and x-ray probe pulses overlapped at the same time on a 0.100 mm × 1.5 mm section of the flowing jet iron complex solution. A volume of 100 ml of this sample was circulated through a metal jet that formed a 100 μm by 2 mm liquid column. It is estimated that only 20% of the 150 μm volume was excited by each excitation pump pulse; therefore, the amount of product formed was negligible compared to the 100 ml total volume. The EXAFS spectra were obtained by exciting the sample with either a 100 fs 267 nm, or 400 nm pulse and monitor the formation and decay of transient structures with a 600 fs hard x-ray continuum pulse, Fig. 1.

The EXAFS spectra of the Fe-O bond change were recorded at 2 ps time intervals between 20 ps before and 100 ps after excitation. Typical EXAFS spectra obtained from Fe(III) oxalate after transformation to μx vs. E at –20 ps (20 ps before excitation) and +25 ps after excitation are reproduced in Fig. 10. The –20 ps spectrum is assigned to the [Fe(III)(C2O4)33-parent molecule before excitation and the +25 ps EXAFS spectrum to a transient species that lives for 25 ps after excitation and subsequently decays to another intermediate which subsequently decays after several milliseconds to from the final Fe(II) product. The μx vs. E spectra were transformed to $|\chi(R)|$ vs. R[Å], that display the Fe-O

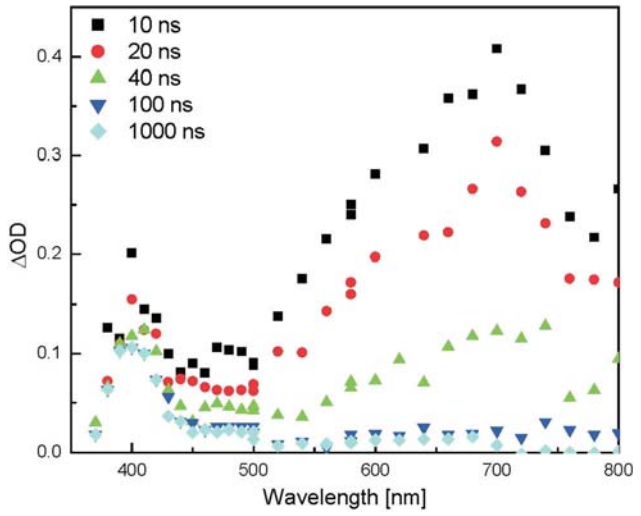

FIG. 8. Nanosecond transient absorption spectra of 2.3×10^{-3} M ferrioxalate in water (266 nm excitation).

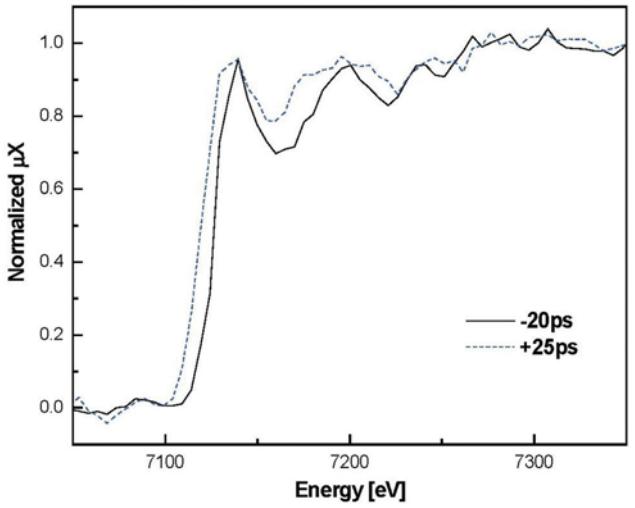

FIG. 10. Fe K-edge x-ray absorption spectra of ferrioxalate/water solution before (solid, −20 ps) and after (point, +25 ps) UV radiation.

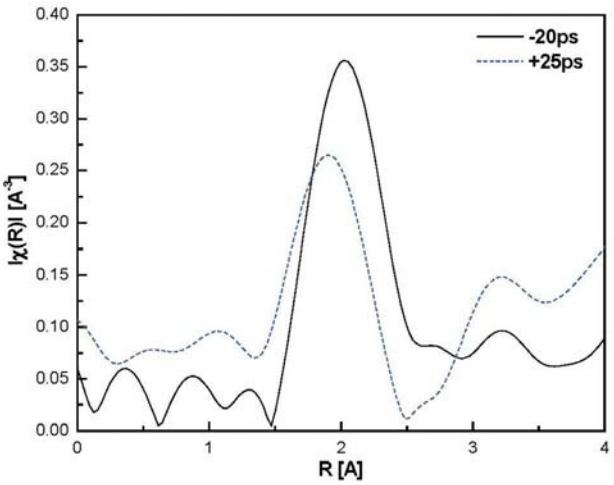

FIG. 11. EXAFS spectra in R space of ferrioxalate/water solution before (solid, −20 ps) and after (point, +25 ps) UV radiation.

bond length as shown in Fig. 11 for two time periods of the electron transfer process: –20 ps and +25 ps. From the $|\chi(R)|$ vs. R spectra, the Fe(III)–O distance was determined to be 2.02 Å for the parent molecule (–20 ps) and 1.84 Å for the transient formed +25 ps after excitation. The values for the Fe(III)–O bond distance measured by the CW x-ray system was determined to be 1.98 Å, which compares very favorably with the 2.00 Å value listed in the literature.[102] Both of these bond lengths are also in very good agreement with the 2.02 Å value obtained, at 20 ps before excitation. The Fe-O bond length at +25 ps after excitation was determined to be 1.84 Å by fs-time resolved EXAFS, which is shorter than the 2.02 Å of parent molecule. We assigned the +25 ps transient to the dissociated Fe(III) complex, $[Fe(III)(C_2O_4)_2^-$ four coordinate transient species. The shorter Fe-O bond length maybe due to the bonding of the iron to four oxalate oxygen atoms instead of the six oxalate oxygen atoms that are bound to the non-excited parent Fe(111) complex. The EXAFS experiments show that the excited state Fe-O bond length is longer than the bond length of the ground state, the parent molecule remains in the excited state during the first 2 ps after excitation, and the (C_2O_4) moiety is intact, yet, electron transfer from Fe(III) complex to Fe(II) complex may have taken place even before dissociation. However, optical data suggest that within 4 ps after excitation dissociation takes place resulting in the formation of the Fe(III) five coordinate Fe(III) intermediate complex. This molecule subsequently dissociates to the four coordinate Fe(III) transient complex measured by time-resolved EXAFS to have a Fe-O bond length of 1.84 Å, and persist for several nanoseconds. Based on this data, this intermediate species was assigned to the same transient that was observed at +25 ps after excitation. Time resolved optical experiments suggested that parent Fe(III) complex reacts with CO_2^- radicals in the nanosecond range, an electron is transferred from CO_2^- to Fe(III) complex to form the Fe(II) complex transient species. Time resolved optical experiments also indicate that several ms after excitation, water is attached to the Fe(II) complex molecule to form a hydrated six coordinated Fe(II)ox complex.

Based on the time resolved optical and EXAFS data presented here and supporting quantum mechanical DFT and H-F calculations, it is proposed that dissociation precedes electron transfer and the photo-induced redox reaction mechanism of Fe(III)ox to Fe(II)ox follows the intermolecular electron transfer mechanism as shown in reactions 1-2. Similar results have been observed for other metal complexes.[18] In essence, this mechanism is supported by: (a) The Fe-O bond distance of the transient intermediate, which was found to be shorter than the Fe(II)-O bond distance of the parent molecule. This strongly supports the proposal that this transient species decay is due to an Fe(III) intermediate rather than the Fe(II) final product. (b) The energy of the exciting photon is sufficient to break both the Fe-O and C-C bonds of the Fe(III) complex to form CO_2^- radicals that subsequently react with and reduce the parent complex via an intermolecular electron transfer mechanism.

It is concluded that electron transfer from Fe(III) complex to Fe(III) in the liquid phase involves a fast dissociation process and proceeds via intermolecular mechanism before intramolecular electron transfer can occur. This process is shown schematically in Fig. 12.

V. TIME RESOLVED XANES

The XANES, x-ray absorption near edge structure, technique is concerned with the region of the x-ray absorption spectrum that lies within ~50 eV of absorption edge and includes the preedge, shown in Fig. 13. The pre-edge region provides information about the oxidation state and bonding characteristics of the system under study, when electrons are promoted to an excited state but not emitted. The x-ray absorption near edge (XANES), also referred to as NEXAFS, is concerned with the region where multiple scattering

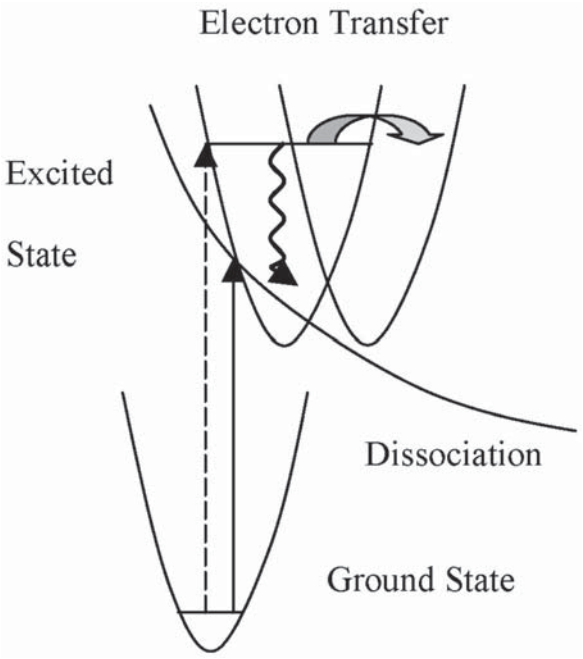

FIG. 12. Schematic diagram of intramolecular electron transfer and intermolecular electron transfer via dissociation mechanism of M(III) complex (L-ligand).

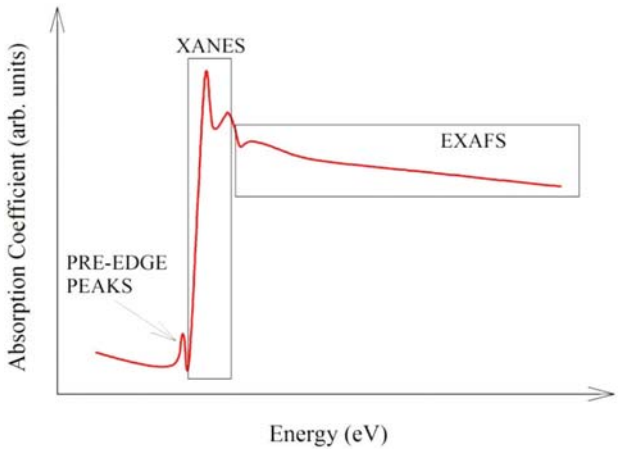

FIG. 13. Schematic representation of x-ray absorption spectra.

becomes dominant and inelastic losses relatively weak. This x-ray absorption region provides information on the local site symmetry, bond length, bond angles, Fermi charge state, and orbital occupancy and a means for one to probe the angular momentum of unoccupied electronic states.

Basically, there is no fundamental distinction between EXAFS and XANES. The different energy ranges in EXAFS and XANES determine which scattering event will be dominant. In XANES, due to its low energy, the wavelength is longer than the interatomic distance, which eventually leads to multiple scattering. However, in EXAFS, unlike XANES, the energy range is much larger and the electron has sufficient kinetic energy to be in the continuum. Therefore the EXAFS wavelength is essentially shorter than the interatomic distance resulting in single scattering events becoming dominant. Although the XANES spectra are simpler and faster to measure than EXAFS, the excitation process that involves multi-electron and multiple scattering make their interpretation more complicated.

XANES spectra techniques have been used widely to determine ground and excited state structures of molecules. The excited state structure provided by XANES (or NEXAFS) which is characteristic of a molecule have found many uses in science and technology including nanoscale distribution of organic compound in soil,[103] monitoring photochemistry of small organic molecules in condensed water and the products produced after irradiation.[104] Also, the evolution of π^* and σ^* transitions with increase in number of graphene layers on a SiO_2 substrate has been studied by means of NEXAFS.[105] In one of several biological studies, adsorption of fibrinogen, the major protein in human plasma, on single-walled carbon nanotubes has been investigated by comparing the NEXAFS spectra before and after fibrinogen treatment.[106] A rather important aspect of XANES spectroscopy is its polarization dependence. Therefore, linearly polarized x-rays have shown to be most suitable for the study of covalent systems such as low-Z molecules, polymers, and macromolecules with directional bonds.[107,108] Lately, NEXAFS spectra of benzene chemisorbed on Ag(110) surface have revealed that when the electric field vector E is normal to the surface, peaks due to the out-of-plane π orbital were seen, whereas in the case of parallel electric field vector, in-plane σ orbital were observed.[109] In this paper, we shall describe briefly two time resolved NEXAFS studies. Time resolved XANES is one of the *in situ* techniques that can produce vast amount of information on many physical processes including electrooxidation of molecular species on metal surfaces such as Pt,[110] the mechanism of fast dynamic catalyzed reactions,[111] and the detection of local structural changes of optically excited ions in solids.[112]

A. Time resolved XANES applied to high spin states mechanism

The population mechanism of the excited high spin quintet state in Iron(II)-based complex has been a long standing issue.[113,114] In a recent study, femtosecond XANES, owing to its ability to probe the molecular structure of the excited states, has been used to identify the elementary steps of the spin crossover dynamics in an iron(II) complex that lead to the formation of the high-spin (HS) quintet state.[16]

To generate the transient spectra from which the fast decaying intermediates were derived, an intense 400-nm (115-fs pulse, at 1 kHz) was used to excite a 100-μm-thick free-flowing liquid jet of an aqueous solution of 50 mM $[Fe^{II}(bpy)_3]^{2+}$. A tunable femtosecond hard x-ray pulse generated by a portion of the slicing source from Swiss light source was used to probe the sample in the transmission mode, at 2 kHz, and a flux of 10 photons per pulse at 7 keV. The transient difference absorption spectra were recorded by alternating the detection of signals between the laser-excited and the unexcited sample. This resulted in an intrinsic energy calibration that compensates for changes in the laser or synchrotron energies and fluxes with a stated time resolution less than 250 fs.

The Fe K-edge XANES spectra of aqueous $[Fe^{II}(bpy)_3]^{2+}$ in its ground (low spin) and excited (high spin) state are shown in Fig. 14(a). The spectrum in Fig. 14(b) (dots) was obtained from the difference between the LS spectrum and the spectrum recorded 50 ps after optical excitation. The arrow in Fig. 14(b), B-feature, shows the strongest increase in absorption when the LS to HS conversion occurs, which was identified as a structure-sensitive above-ionization multiple scattering resonances.[115] There is a direct dependence between the increase in intensity of the B-feature and the increase in Fe-N bond distance upon LS to HS conversion, reflecting a well-established correlation between edge absorption intensity and bond distance. This correlation was also confirmed by a computer simulation of the XANES spectrum using the Minuit XANES (MXAN) code,[116,117] which additionally shows a nearly linear relationship between the Fe-N bond elongation and the intensity of the B-feature. The B-feature intensity, based on this data, was attributed to the Fe-N bond elongation makes possible to distinguish the various states that can be grouped by similar Fe-N bond distances: (i) the LS ground and the 1,3 MLCT states; (ii) the 1,3 T states, which exhibit an elongation of 0.1 Å relative to the ground state; and (iii) the 5 T state, which exhibits a 0.2 Å elongation. The transient signal at the B-feature was obtained as a function of delay which shows that there is a steep increase up to ~300 fs followed

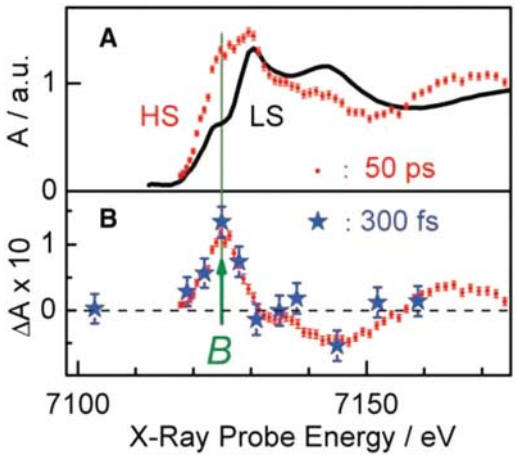

FIG. 14. Fe K-edge XANES spectrum of the LS state of aqueous [FeII(bpy)3]2+ (black trace) and of the HS quintet state (red dots). (B) Transient XANES spectrum (difference in x-ray absorption between the laser-excited sample and the unexcited sample) recorded 50 ps after laser excitation at 400 nm (red dots) (11). The blue stars represent the transient spectrum recorded at a time delay of 300 fs in the present work. Reprinted with permission from C. Bressler, C. Milne, V. T. Pham, A. ElNahhas, R. M. van der Veen, W. Gawelda, S. Johnson, P. Beaud, G. Grolimund, M. Kaiser, C. N. Borca, G. Ingold, R. Abela, M. Chergui, Science **323**, 489–92 (2009). Copyright © 2009.[16]

by a plateau beyond 300 fs, which implies that system has already reached the HS state. This was confirmed by a similar transient absorption spectrum recorded at 50-ps delay at a time delay of 300 fs, depicted by stars in Fig. 14(b).

Comparison of the simulated and experimental data suggested that (~150 fs) rise time of the HS state x-ray absorption is due to MLCT, which implies that the population of the MLCT proceeds directly to quintet state and bypasses the intermediate states. In addition, the data indicate that the derived relaxation time scale corresponds to the period of the Fe-N stretch mode. Essentially, this experiment is rather typical of XANES that reveal the structural dynamics, the population relaxation pathways and mechanism responsible for the population of the excited high spin state.

B. Time resolved XANES applied to solar cells

Photovoltaic devices, solar cells, have been dominated by silicon based semiconductor materials owing to the fact that silicon has an intrinsic bandgap that absorbs solar radiation; it is abundant, can be easily obtained pure and, is inexpensive. Lately, alternative solar cell systems have emerged. One of them is based on TiO_2 which has wider bandgap than Si.[118] Because, TiO_2 absorbs only higher energy solar light, it must be coupled to organic dyes that absorb lower energy solar radiation. One of the most common and efficient is ruthenium based dyes. The Ruthenium dye absorbs solar photons which eject electrons from the dye that are injected into the conduction band of TiO_2 semiconductor. The ejected electron of the dye must be regenerated by electron transfer from a redox species contained in the system in order to complete the circuit. Such systems, based on metal oxides and organic dye molecules are usually referred to as dye-sensitized solar cells (DSSCs). The rational design of solar cell requires understanding of all materials at the molecular level and knowledge of the structural reorganization of interfacial charge transfer that drives the solar cell reaction between the transition-metal complex dye molecules and semiconductor nanoparticles. The structural evolution of the dye sensitizer and rearrangement of the nanocrystals surface associated with the electron density shift during and after interfacial charge injection has been to a large extend studied theoretically.[119–121] Recent x-ray transient absorption spectroscopy studies have reported on the transient electronic and geometric structures of a ruthenium complex dye sensitizer adsorbed to TiO_2 nanoparticles surfaces developed while the solar cell is undergoing interfacial photoinduced charge separation.[122]

In x-ray absorption experiments, TiO_2 nanoparticles, prepared by the sol gel method, were added to RuN3 in methanol solution. The X-ray transient absorption (XTA) experiments were carried out at the Advanced Photon source of the Argonne National Laboratory. The laser pump pulse was the 527 nm, 5 ps second harmonic pulse output of Nd:YLF at 1 kHz repetition rate. X-ray probe pulses were derived from electron bunches extracted from the storage ring with 80 ps FWHM and 6.5 MHz repetition rate. The laser and x-ray probe pulses intersected a flowing sample stream of highly dispersed RuN3 (0.7 mM)-sensitized TiO_2 nanoparticles suspended in ethanol with continuous purging with dry nitrogen gas and circulated by a peristaltic pump. The delay between pump and probe pulses were adjusted by using a programmable delay line. Two photomultiplier tubes (PMTs) coupled to plastic scintillators were used at 90° angle on both sides to the incident x-ray beam to collect the x-ray fluorescence signal.

Figure 15 displays the XANES spectra measured at the Ru K-edge with and without laser excitation at a delay time of 50 ps after the laser pump pulse. At this delay time, the photoexcited RuN3 molecules are thought to be mostly in the oxidized form, $Ru^{III}N3^+$, which is in agreement with previous studies and optical transient absorption (OTA) measurements under the same conditions. The absorption edge energy of the laser-on XANES spectrum is slightly

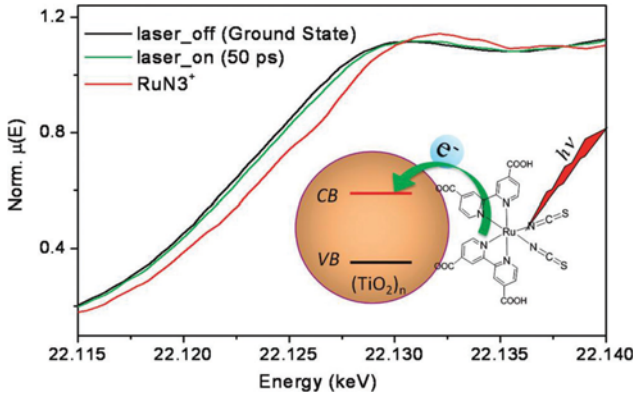

FIG. 15. XANES spectra of RuN3 adsorbed to TiO_2 nanoparticle surface measured at Ru K-edge. The black and green curves are spectra without the laser and with laser excitation at nominally 50 ps, respectively. The red curve is the spectrum for the charge separate state, $RuN3^+$, extracted from the green curve with a 20% conversion at the 50 ps delay. Inset: schematic of MLCT excitation of RuN3, followed by interfacial electron injection from excited RuN3 to TiO_2 nanoparticle. Reprinted with permission from X. Zhang, G. Smolentsev, J. Guo, K. Attenkofer, C. Kurtz, G. Jennings, J. V. Lockard, A. B. Stickrath, L. X. Chen, J. Phys. Chem. Lett. **2**, 628–632 (2011). Copyright © 2011.[122]

up-shifted by ~0.23 eV, as expected for $Ru^{III}N3^{+}$ due to an effectively higher oxidation state of the Ru center after the photoinduced electron injection into the TiO_2 lattice.

These results show that the conversion from the ground to the charge-separate states causes different responses on the Ru-N bonds with different ligands. Upon the conversion from the ground-state RuN3/TiO_2 to $RuN3^{+}/TiO_2^{-}$, the average Ru-N(NCS) bond length shortens by ~0.06 Å, from 2.05 to 1.99 Å, whereas the average Ru-N (dcbpy) bond length shows practically no changes.

The structural changes of RuN3 dye adsorbed onto a TiO_2 nanoparticle surface that accompany the photoinduced electron injection from the dye to TiO_2 were measured using x-ray transient absorption and multidimensional interpolation analysis. The results show that the average Ru-NCS bond length reduces by 0.06 Å, whereas the average Ru-N(dcbpy) bond length remains nearly unchanged after the electron injection. In addition, different responses in the Ru-N bonds with dcbpy and NCS ligands to the photoinduced electron injection have been directly characterized. It is believed that the detailed transient structures obtained from this work could provide guidance in selecting ligands for the dye sensitizer and for theoretical modeling of molecular orbital energetic in DSSCs processes.

VI. CONCLUSION

The described experiments in this article were aimed at demonstrating that time resolved x-ray techniques provide a powerful means for obtaining new data and knowledge on the structure of short-lived excited states and transient species that were not available previously. Now, by combining ultrafast optical electron and x-ray pulses, it is expected that scientist will be able to determine global histograms of the ultrafast phenomena, processes, and transients that determine the course, and affect the final product of an excitation processes in solids and liquids.

The major disadvantages of table-top x-ray sources are their rather weak intensity and the low repetition rate. The repetition rate has been improved and now can generate femtosecond pulses x-ray pulses at 10 kHz rate. However, the energy is very low. At the present time new systems are been developed that are based on x-ray diode principle that promise to increase the both the repetition rate and the energy of the subpicosecond pulses. Applications of the new table-top x-ray system include single molecule ground state and excited state structures, intramolecular electron and proton hopping in biological molecules and the possibility of the development of a hard x-ray laser.

ACKNOWLEDGMENTS

This work was supported in part by The W. M. Keck Foundation. J.C. also thanks the National Natural Science Foundation of China under Grants Nos. 11004132, 10734130, and 10874113 and the National Basic Research Program of China under Grant No. 2007CB815101.

[1]I. V. Tomov, T. Anderson, and P. M. Rentzepis, "Picosecond x-ray pulses generated in a diode driven by 193-nm picosecond laser pulses," J. X-ray Sci.Technol. **4**, 44–56 (1993).
[2]I. V. Tomov, P. Chen, and P. M. Rentzepis, "Nanosecond hard x-ray source for time resolved x-ray diffraction studies," Rev. Sci. Instrum. **66**, 5214–5217 (1995).
[3]H. E. Elsayed-Ali and G. A. Mourou, "Picosecond reflection high-energy electron diffraction," Appl. Phys. Lett. **52**, 103–104 (1988).
[4]H. Ihee, V. A. Lobastov, U. M. Gomez, B. M. Goodson, R. Srinivasan, C.-Y. Ruan, and A. H. Zewail, "Direct imaging of transient molecular structures with ultrafast diffraction," Science **291**, 458–462 (2001).
[5]P. M. Rentzepis, "Emission from the lowest singlet and triplet states of azulene," Chem. Phys. Lett. **3**, 717–720 (1969).
[6]T. Feurer, A. Morak, I. Uschmann, C. Ziener, H. Schwoerer, E. Forster, and R. Sauerbrey, "An incoherent sub-picosecond x-ray source for time-resolved x-ray-diffraction experiments," Appl. Phys. B **72**, 15–20 (2001).
[7]L. X. Chen, "Probing transient molecular structures in photochemical processes using laser-initiated time-resolved x-ray absorption spectroscopy," Ann. Rev. Phys. Chem. **56**, 221–254 (2005).
[8]F. Raksi, K. R. Wilson, Z. M. Jiang, A. Ikhlef, C. Y. Cote, and J. C. Kieffer, "Ultrafast x-ray absorption probing of a chemical reaction," J. Chem. Phys. **104**, 6066–6069 (1996).
[9]M. Saes, C. Bressler, R. Abela, D. Grolimund, S. L. Johnson, P. A. Heimann, and M. Chergui, "Observing photochemical transients by ultrafast x-ray absorption spectroscopy," Phys. Rev. Lett. **90**, 047403–4 (2003).
[10]T. Lee, Y. Jiang, C. G. Rose-Petruck, and F. Benesch, "Ultrafast tabletop laser-pump–x-ray probe measurement of solvated Fe(CN)64−," J. Chem. Phys. **122**, 084506 (2005).
[11]M. Khalil, M. A. Marcus, A. L. Smeigh, J. K. McCusker, H. H. W. Chong, and R. W. Schoenlein, "Picosecond x-ray absorption spectroscopy of a photoinduced iron(II) spin crossover reaction in solution," J. Phys. Chem. A **110**, 38–44 (2006).
[12]K. Oguri, Y. Okano, T. Nishikawa, and H. Nakano, "Dynamics of femtosecond laser ablation studied with time-resolved x-ray absorption fine structure imaging," Phys. Rev. B **79**, 144106–10 (2009).
[13]H. Ihee, "Visualizing solution-phase reaction dynamics with time-resolved x-ray liquidography," Acc. Chem. Soc. **42**, 356–366 (2008).
[14]M. Lorenc, J. Hébert, N. Moisan, E. Trzop, M. Servol,M. Buron-Le Cointe, H. Cailleau, M. L. Boillot, E. Pontecorvo, M. Wulff, S. Koshihara, and E. Collet, "Successive dynamical steps of photoinduced switching of a molecular Fe(III) spin-crossover material by time-resolved x-ray diffraction," Phys. Rev. Lett. **103**, 028301–4 (2009).
[15]K. Alexopoulos, M. Anilkumar, M.-F. Reyniers, H. Poelman, S. Cristol, V. Balcaen, P. M. Heynderickx, D. Poelman, and G. B. Marin, "Time-resolved operando X-ray absorption study of CuO–CeO2/Al2O3 catalyst during total oxidation of propane," Appl. Catal. B **97**, 381–388 (2010).
[16]C. Bressler, C. Milne, V. T. Pham, A. ElNahhas, R. M. van der Veen, W. Gawelda, S. Johnson, P. Beaud, G. Grolimund, M. Kaiser, C. N. Borca, G. Ingold, R. Abela, and M. Chergui, "Femtosecond XANES study of the light-induced spin crossover dynamics in an iron(II) complex," Science **323**, 489–92 (2009).
[17]H. Zhang, J. Chen, I. V. Tomov, A. S. Dvornikov, and P. M. Rentzepis, "Photoelectron detachment and solvated electron dynamics of the cobalt(III) and iron(III) oxalato complexes," J. Phys. Chem. A **111**, 11584–11588 (2007).
[18]J. Chen, H. Zhang, I. V. Tomov, and P. M. Rentzepis, "Laser induced transient structures in a 150 nm gold crystal," J. Chin. Chem Soc. **54**, 1619–1628 (2007).
[19]H.E. Elsayed-Ali, T. B. Norris, M. A. Pessot, and G. A. Mourou, "Time-resolved observation of electron-phonon relaxation in copper," Phys. Rev. Lett. **58**, 1212–1215 (1987).
[20]J. W. Herman, H. E. Elsayed-Ali, and E. A. Murphy, "Time-resolved structural study of Pb(100)," Phys. Rev. Lett. **71**, 400–403 (1993).
[21]J. Cao, Y. Gao, H. E. Elsayed-Ali, R. J. D. Miller, and D. A. Mantell, "Femtosecond photoemission study of ultrafast electron dynamics in single-crystal Au(111) films," Phys. Rev. B **58**, 10948–10952 (1998).
[22]C. A. Schmuttenmaer, M. Aeschlimann, H. E. Elsayed-Ali, R. J. D. Miller, D. A. Mantell, J. Cao, and Y. Gao, "Time-resolved two-photon photoemission from Cu(100): Energy dependence of electron relaxation," Phys. Rev. B **50**, 8957–8960 (1994).
[23]M. Aeschlimann, C. A. Schmuttenmaer, H. E. Elsayed-Ali, R. J. D. Miller, J. Cao,Y. Gao, and D. A. Mantell, "Observation of surface enhanced multiphoton photoemission from metal surfaces in the short pulse limit," J. Chem. Phys. **102**, 8606–8613 (1995).
[24]J. Chen, W.-K. Chen, J. Tang, and P. M. Rentzepis, "Time-resolved structural dynamics of thin metal films heated with femtosecond optical pulses," PNAS **108**, 18887–18892 (2011).

[25]J. Chen, I. V. Tomov, H. E. Elsayed-Ali, and P. M. Rentzepis, "Hot electrons blast wave generated by femtosecond laser pulses on thin Au(111) crystal, monitored by subpicosecond x-ray diffraction," Chem. Phys. Lett. **419**, 374–378 (2006).
[26]Z.-H. Loh, M. Khalil, R. E. Correa, and S. R. Leone, "A tabletop femtosecond time-resolved soft x-ray transient absorption spectrometer," Rev. Sci. Instrum. **79**, 073101–13 (2008).
[27]M. Harb, R. Ernstorfer, C. T. Hebeisen, G. Sciaini, W. Peng, T. Dartigalongue, M. A. Eriksson, M. G. Lagally, S. G. Kruglik, and R. J. D. Miller, "Electronically driven structure changes of si captured by femtosecond electron diffraction," Phys. Rev. Lett. **100**, 155504–4 (2008).
[28]A. A. Ischenko, V. P. Spiridonov, L. Schäfer, and J. D. Ewbank, "The stroboscopic gas electron diffraction method for investigation of time-resolved structural kinetics in photoexcitation processes," J. Mol. Struct. **300**, 115–140 (1993).
[29]V. A. Lobastov, J. D. Ewbank, L. Schafer, and A. A. Ischenko, "Instrumentation for time-resolved electron diffraction spanning the time domain from microseconds to picoseconds," Rev. Sci. Instrum. **69**, 2633–2643 (1998).
[30]L. Schafer, "Electron diffraction studies of free radicals. I. Indenyl," J. Am. Chem. Soc. **90**, 3919–3925 (1968).
[31]A. Oguz Er, J. Chen, J. Tang, and P. M. Rentzepis, "Coherent acoustic wave oscillations and melting on Ag(111) surface by time resolved x-ray diffraction," Appl. Phys. Lett. **100**, 151910–5 (2012).
[32]J. R. Helliwell and P. M. Rentzepis, *Time Resolved Diffraction* (Oxford University Press, Oxford, 1997).
[33]K. Agarval, *X-ray Spectroscopy* (Springer, New York, 1991).
[34]A. Rousse, C. Rischel, and J. C. Gauthier, "Colloquium: femtosecond x-ray crystallography," Rev. Mod. Phys. **73**, 17–31 (2001).
[35]C. Bressler and M. Chergui, "Ultrafast x-ray absorption spectroscopy," Chem. Rev. **104**, 1781–1812 (2004).
[36]M. A. Kumakhov and F. F. Komarov, "Multiple reflection from surface x-ray optics," Phys. Rep. **191**, 289–350 (1990).
[37]I. V. Tomov, J. Chen, X. Ding, and P. M. Rentzepis, "Efficient focusing of hard X-rays generated by femtosecond laser driven plasma," Chem. Phys. Lett. **389**, 363–369 (2004).
[38]M. Bargheer, N. Zhavoronkov, Y. Gritsai, J. C. Woo, D. S. Kim, M. Woerner, and T. Elsaesser, "Coherent atomic motions in a nanostructure studied by femtosecond x-ray diffraction," Science **306**, 1771–1773 (2004).
[39]A. Rindby, "Progress in x-ray microbeam spectrometry," X-Ray Spectrom. **22**, 187–191 (1993).
[40]D. Von Der Linde and K. Sokolowski-tinten, "X-ray diffraction experiments with femtosecond time resolution," J. Mod. Phys. **50**, 683–694 (2003).
[41]K. Sokolowski-Tinten, C. Blome, C. Dietrich, A. Tarasevitch, M. Horn von Hoegen, D. von der Linde, A. Cavalleri, J. Squier, and M. Kammler, "Femtosecond x-ray measurement of ultrafast melting and large acoustic transients," Phys. Rev. Lett. **87**, 225701–4 (2001).
[42]K. Sokolowski-Tinten, J. Bialkowski, and D. von der Linde, "Ultrafast laser-induced order-disorder transitions in semiconductors," Phys. Rev. B **51**, 14186–14198 (1995).
[43]C. Thomsen, H. T. Grahn, H. J. Maris, and J. Tauc, "Surface generation and detection of phonons by picosecond light pulses," Phys. Rev. B **34**, 4129–4138 (1986).
[44]V. E. Gusev, "On the duration of acoustic pulses excited by subpicosecond laser action on metals," Opt. Commun. **94**, 76–78 (1992).
[45]O. B. Wright, "Ultrafast nonequilibrium stress generation in gold and silver," Phys. Rev. B **49**, 9985–9988 (1994).
[46]M. Nisoli, S. De Silvestri, A. Cavalleri, A. M. Malvezzi, A. Stella, G. Lanzani, P. Cheyssac, and R. Kofman, "Coherent acoustic oscillations in metallic nanoparticles generated with femtosecond optical pulses," Phys. Rev. B **55**, R13424–R13427 (1997).
[47]H. Park, X. Wang, S. Nie, R. Clinite, and J. Cao, "Mechanism of coherent acoustic phonon generation under nonequilibrium conditions," Phys. Rev. B **72**, 100301(R)–4 (2005).
[48]M. Hada, K. Okimura, and J. Matsuo, "Photo-induced lattice softening of excited-state VO[sub 2]," Appl. Phys. Lett. **99**, 051903–3 (2011).
[49]A. M. Linderberg, I. Kang, S. L. Johnson, T. Missalla, P. A. Heimann, Z. Chang, J. Larson, P. H. Bucksbaum, H. C. kapteyn, H. A. Padmore, R. W. Lee, J. S. Wark, and R. W. Falcone, "Time resolved x-ray diffraction during a laser induced phase transistion," Phys. Rev. Lett. **84**, 111–114 (2000).
[50]L. A. Falkovsky and E. G. Mishchenko, "Electron-lattice kinetics of metals heated by ultrashort laser pulses," JETP **88**, 84–88 (1999).
[51]D. Y. Tzou, J. K. Chen, and J. E. Beraun, in 2001 IMECE, New York, 2001.
[52]J. K. Chen, J. E. Beraun, L. E. Grames, and D. Y. Tzou, "Short-time thermal effects on thermomechanical response caused by pulsed lasers," J. Thermophys. Heat Transfer **17**, 35–42 (2003).
[53]P. Musumeci, J. T. Moody, C. M. Scoby, M. S. Gutierrez, and M. Westfall, "Laser-induced melting of a single crystal gold sample by time-resolved ultrafast relativistic electron diffraction," Appl. Phys. Lett. **97**, 063502–3 (2010).
[54]Y. Gan and J. K. Chen, "Thermomechanical wave propagation in gold films induced by ultrashort laser pulses," Mech. Mater. **42**, 491–501 (2010).
[55]J. Chen and P. M. Rentzepis, in *Advances in Multi-photon Processes and Spectroscopy*, edited by S. H. Lin, A. A. Villaeys, and Y. Fujimura (World Scientific, Singapore, 2010), Vol. 19, pp. 117–183.
[56]D. Shorokhov and A. H. Zewail, "4D electron imaging: principles and perspectives," Phys. Chem. Chem. Phys. **10**, 2879 (2008).
[57]J. Hohlfeld, S. S. Wellershoff, J. Gudde, U. Conrad, V. Jahnke, and E. Matthias, "Electron and lattice dynamics following optical excitation of metals," Chem. Phys. **251**, 237–258 (2000).
[58]L. X. Chen, W. J. H. Jager, G. Jennings, D. J. Gosztola, A. Munkholm, and J. P. Hessler, "Capturing a photoexcited molecular structure through time-domain x-ray absorption fine structure," Science **292**, 262–264 (2001).
[59]J. Tang, "Coherent phonon excitation and linear thermal expansion in structural dynamics and ultrafast electron diffraction of laser-heated metals," J. Chem. Phys. **128**, 164702–14 (2008).
[60]P. Yu, J. Tang, and S.-H. Lin, "Photoinduced structural dynamics in laser-heated nanomaterials of various shapes and sizes," J. Phys. Chem. C **112**, 17133–17137 (2008).
[61]A. Cavalleri, C. W. Siders, F. L. H. Brown, D. M. Leitner, C. Tóth, J. A. Squier, C. P. J. Barty, K. R. Wilson, K. Sokolowski-Tinten, M. Horn von Hoegen, D. von der Linde, and M. Kammler, "Anharmonic lattice dynamics in germanium measured with ultrafast x-ray diffraction," Phys. Rev. Lett. **85**, 586–589 (2000).
[62]M. Nicoul, U. Shymanovich, A. Tarasevitch, D. von der Linde, and K. Sokolowski-Tinten, "Picosecond acoustic response of a laser-heated gold-film studied with time-resolved x-ray diffraction," Appl. Phys. Lett. **98**, 191902–3 (2011).
[63]J. R. Dwyer, C. T. Hebeisen, R. Ernstorfer, M. Harb, V. B. Deyirmenjian, R. E. Jordan, and R. J. D. Miller, "Femtosecond electron diffraction: 'making the molecular movie," Philos. Trans. R. Soc. A **364**, 741–778 (2006).
[64]N. Bonini, M. Lazzeri, N. Marzari, and F. Mauri, "Phonon anharmonicities in graphite and graphene," Phys. Rev. Lett. **99**, 176802–4 (2007).
[65]S. Narasimhan and D. Vanderbilt, "Anharmonic self-energies of phonons in silicon," Phys. Rev. B **43**, 4541–4544 (1991).
[66]W.-L. Chan, R. S. Averback, D. G. Cahill, and A. Lagoutchev, "Dynamics of femtosecond laser-induced melting of silver," Phys. Rev. B **78**, 214107–8 (2008).
[67]D. M. Fritz, D. A. Reis, B. Adams, R. A. Akre, J. Arthur, C. Blome, P. H. Bucksbaum, A. L. Cavalieri, S. Engemann, S. Fahy, R. W. Falcone, P. H. Fuoss, K. J. Gaffney, M. J. George, J. Hajdu, M. P. Hertlein, P. B. Hillyard, M. Horn-von Hoegen, M. Kammler, J. Kaspar, R. Kienberger, P. Krejcik, S. H. Lee, A. M. Lindenberg, B. McFarland, D. Meyer, T. Montagne, E. D. Murray, A. J. Nelson, M. Nicoul, R. Pahl, K. Rudati, H. Schlarb, D. P. Siddons, K. Sokolowski-Tinten, T. Tschentscher, D. von der Linde, and J. B. Hastings, "Ultrafast bond softening in bismuth: mapping a solid's interatomic potential with x-rays," Science **315**, 633–636 (2007).
[68]F. Schotte, J. Soman, J. S. Olson, M. Wulff, and P. A. Anfinrud, "Picosecond time-resolved X-ray crystallography: probing protein function in real time," J. Struct. Biol. **147**, 235–246 (2004).
[69]F. Schotte, M. Lim, T. A. Jackson, A. V. Smirnov, J. Soman, J. S. Olson, G. N. Phillips, M. Wulff, and P. A. Anfinrud, "Watching a protein as it functions with 150-ps time-resolved x-ray crystallography," Science **300**, 1944–1947 (2003).
[70]J. Kim, K. H. Kim, J. G. Kim, T. W. Kim, Y. Kim, and H. Ihee, "Anisotropic picosecond x-ray solution scattering from photoselectively aligned protein molecules," J. Phys. Chem. Lett. **2**, 350–356 (2011).
[71]L. Young, E. P. Kanter, B. Krässig, Y. Li, A. M. March, S. T. Pratt, R. Santra, S. H. Southworth, N. Rohringer, L. F. DiMauro, G. Doumy, C. A. Roedig, N. Berrah, L. Fang, M. Hoener, P. H. Bucksbaum, J. P. Cryan, S. Ghimire, J. M. Glownia, D. A. Reis, J. D. Bozek, C. Bostedt, and M. Messerschmidt, "Femtosecond electronic response of atoms to ultra-intense x-rays," Nature **466**, 56–61 (2010).

[72]S. M. Vinko, O. Ciricosta, B. I. Cho, K. Engelhorn, H. K. Chung, C. R. D. Brown, T. Burian, T. J. Chalupsky, R. W. Falcone, C. Graves, V. Hajkova, A. Higginbotham, L. Juha, J. Krzywinski, H. J. Lee, M. Messerschmidt, C. D. Murphy, Y. Ping, A. Scherz, W. Schlotter, S. Toleikis, J. J. Turner, L. Vysin, T. Wang, B. Wu, U. Zastrau, D. Zhu, R. W. Lee, P. A. Heimann, B. Nagler, and J. S. Wark, "Creation and diagnosis of a solid-density plasma with an x-ray free-electron laser," Nature **482**, 59–62 (2012).
[73]N. Rohringer, D. Ryan, R. A. London, M. Purvis, F. Albert, J. Dunn, J. D. Bozek, C. Bostedt, A. Graf, R. Hill, S. P. Hau-Riege, and J. J. Rocca, "Atomic inner-shell x-ray laser at 1.46 nanometres pumped by an x-ray free-electron laser," Nature **481**, 488–491 (2012).
[74]L. Lomb, T. R. M. Barends, S. Kassemeyer, A. Aquila, S. W. Epp, B. Erk, L. Foucar, R. Hartmann, B. Rudek, D. Rolles, A. Rudenko, R. L. Shoeman, J. Andreasson, S. Bajt, M. Barthelmess, A. Barty, M. J. Bogan, C. Bostedt, J. D. Bozek, C. Caleman, R. Coffee, N. Coppola, D. P. DePonte, R. B. Doak, T. Ekeberg, H. Fleckenstein, P. Fromme, M. Gebhardt, H. Graafsma, L. Gumprecht, C. Y. Hampton, A. Hartmann, G. Hauser, H. Hirsemann, P. Holl, J. M. Holton, M. S. Hunter, W. Kabsch, N. Kimmel, R. A. Kirian, M. Liang, F. R. N. C. Maia, A. Meinhart, S. Marchesini, A. V. Martin, K. Nass, C. Reich, J. Schulz, M. M. Seibert, R. Sierra, H. Soltau, J. C. H. Spence, J. Steinbrener, F. Stellato, S. Stern, N. Timneanu, X. Wang, G. Weidenspointner, U. Weierstall, T. A.White, C. Wunderer, H. Chapman, J. Ullrich, L. Strüder, I. Schlichting, "Radiation damage in protein serial femtosecond crystallography using an x-ray free-electron laser," Phys. Rev. B **84**, 214111–6 (2011).
[75]S. Adachi, J. Kim, H. Ihee, "Synchrotron-based time-resolved x-ray solution scattering (liquidography)," *Advances in Lasers and Electro Optics*, edited by Nelson Costa and Adolfo Cartaxo (Intech, 2010).
[76]T. K. Kim, J. H. Lee, M. Wulff, Q. Kong, and H. Ihee, "Spatiotemporal kinetics in solution studied by time-resolved x-ray liquidography (solution scattering)," ChemPhysChem **10**, 1958–1980 (2009).
[77]S. Jun, J. H. Lee, J. Kim, J. Kim, K. H. Kim, Q. Kong, T. K. Kim, M. Lo Russo, M. Wulff, and H. Ihee, "Photochemistry of $HgBr_2$ in methanol investigated using time-resolved X-ray liquidography," Phys. Chem. Chem. Phys. **12**, 11536–11547 (2010).
[78]M. Christensen, K. Haldrup, K. Bechgaard, R. Feidenhans'l, Q. Y. Kong, M. Cammarata, and M. Wulff M. Lo Russo, N. Harrit, and M. M. Nielsen, J. Am. Chem. Soc. **131**, 502–508 (2009).
[79]J. Kim, J. H. Lee, J. Kim, S. Jun, K. H. Kim, T. W. Kim, M. Wulff, and H. Ihee, "Structural dynamics of 1,2-diiodoethane in cyclohexane probed by picosecond x-ray liquidography," J. Phys. Chem. A **116**, 2713–2722 (2011).
[80]S. Ibrahimkutty, J. Kim, M. Cammarata, F. Ewald, J. Choi, H. Ihee, and A. Plech, "Ultrafast structural dynamics of the photocleavage of protein hybrid nanoparticles," ACS Nano **5**, 3788–3794 (2011).
[81]H. B. Gray and B. G. Malmström, "On the relationship between protein-forced ligand fields and the properties of blue copper centers," Comments Inorg. Chem. **2**, 203–209 (1983).
[82]P. S. Mariano, *Advances in Electron Transfer Chemistry* (JAI, Stanford, CT, 1999) Vol. 6.
[83]Proton Transfer, edited by C. H. Bamford and C. H. F. Tipper (Elsevier, Oxford, 1977) Vol. 17.
[84]M. Kondo, I. A. Heisler, D. Stoner-Ma, P. J. Tonge, and S. R. Meech, "Ultrafast dynamics of protein proton transfer on short hydrogen bond potential energy surfaces: S65T/H148D GFP," J. Am. Chem. Soc. **132**, 1452–1453 (2010).
[85]A. O. Er and H. E. Elsayed-Ali, "Electronically enhanced surface diffusion during Ge growth on Si(100)," J. Appl. Phys. **109**, 084320–6 (2011).
[86]A. O. Er, W. Ren, and H. Elsayed-Ali, "Low temperature epitaxial growth of Ge quantum dot on Si(100)-(2×1) by femtosecond laser excitation," Appl. Phys. Lett. **98**, 013108–3 (2011).
[87]T. Pfeifer, C. Spielmann, and G. Gerber, "Femtosecond x-ray science," Rep. Prog. Phys. **69**, 443–505 (2006).
[88]W. G. Palmer, *Experimental Inorganic Chemistry* (University Press, Cambridge, 1970).
[89]V. Balzani and V. Carassiti, *Photochemistry of Coordination Compounds* (Academic Inc., New York, 1970).
[90]C. K. Jorgensen, "Spectroscopy of transition-group complexes," Adv. Chem. Phys. **5**, 33–146 (1963).
[91]T. B. Copestake and N. Uri, "The photochemistry of complex ions—photochemical and thermal decomposition of the trioxalatocobaltate-III complex," Proc. R. Soc. A **228**, 252–263 (1955).
[92]J. N. Cooper, H. L. Hoyt, C. Buffingt, and C. A. Holmes, "Oxidation of hypophosphorous acid by vanadium(V)," J. Phys. Chem. **75**, 891–894 (1971).
[93]A. J. Allmand and W. W. Webb, "CXCVII.-The photolysis of potassium ferrioxalate solutions. Part I. Experimental," J. Chem. Soc. 1518–1531 (1929).
[94]R. Livingston, "The photochemical oxidation of oxalic acid sensitized by ferric ion," J. Phys. Chem. **44**, 601–611 (1940).
[95]C. A. Parker, A new sensitive chemical actinometer.1. some trials with potassium ferrioxalate," Proc. R. Soc. A **220**, 104–116 (1953).
[96]C. G. Hatchard and C. A. Parker, "A new sensitive chemical actinometer. 2. Potassium ferrioxalate as a standard chemical actinometer," Proc. R. Soc. A **235**, 518–536 (1956).
[97]R. A. Horne, The kinetics of the oxalate catalysis of the iron(II)-iron(III) electron-exchange reaction in aqueous solution," J. Phys. Chem. **64**, 1512–1517 (1960).
[98]J. H. Baxendale, C. Capellos, E. J. Land, J. P. Keene, M. Ebert, A. J. Swallow, J. V. Davies, J. M. Francis, C. W. Gilbert, E. M. Fielden, and J. M. Nosworthy, "Pulse radiolysis," Nature **201**, 468–470 (1964).
[99]S. Pommeret, R. Naskrecki, P. van der Meulen, M. Menard, G. Vigneron, and T. Gustavsson, "Ultrafast events in the electron photodetachment from the hexacyanoferrate(II) complex in solution," Chem. Phys. Lett. **288**, 833–840 (1998).
[100]J. M. Wiesenfeld and E. P. Ippen, "Dynamics of electron solvation in liquid water," Chem. Phys. Lett. **73**, 47–50 (1980).
[101]C. D. Jonah, J. R. Miller, E. J. Hart, and M. S. Matheson, "Picosecond pulse-radiolysis. 1. Time or concentration dependent rate constants," J. Phys. Chem. **79**, 2705–2711 (1975).
[102]E. H. Merrachi, B. F. Mentzen, F. Chassagneux, and J. Bouix, "Crystal-chemistry of monovaent-cation trisoxalatometallates(III). 2. $(NH_4)_3FE(C_20_4)_{3\cdot3}H_2O$," Rev. Chim. Miner. **24**, 56–57 (1987).
[103]J. Lehmann, B. Q. Liang, D. Solomon, M. Lerotic, F. Luizao, J. Kinyangi, T. Schafer, S. Wirick, and C. Jacobsen, "Near-edge x-ray absorption fine structure (NEXAFS) spectroscopy for mapping nano-scale distribution of organic carbon forms in soil: Application to black carbon particles," Global Biogeochem. Cycles **19**, GB1013–12 (2005).
[104]P. Parent, C. Laffon, F. Bournel, J. Lasne, and S. Lacombe, "NEXAFS: a unique tool to follow the photochemistry of small organic molecules in condensed water," J. Phys.:Conf. Ser. **261**, 012008–7 (2011).
[105]D. Pacilé, M. Papagno, A. F. Rodríguez, M. Grioni, L. Papagno, C. O. Girit, J. C. Meyer, G. E. Begtrup, and A. Zettl, "Near-edge x-ray absorption fine-structure investigation of graphene," Phys. Rev. Lett. **101**, 066806–4 (2008).
[106]L. Song, J. Meng, J. Zhong, L. Liu, X. Dou, D. Liu, X. Zhao, S. Luo, Z. Zhang, Y. Xiang, H. Xu, W. Zhou, Z. Wu, and S. Xie, "Human fibrinogen adsorption onto single-walled carbon nanotube films," Colloids Surf. B **49**, 66–70 (2006).
[107]J. Stöhr and H. C. Siegmann, *Magnetism* (Springer, 2006).
[108]P. Guttmann, C. Bittencourt, S. Rehbein, P. Umek, X. Ke, G. Van Tendeloo, C. P. Ewels, and G. Schneider, "Nanoscale spectroscopy with polarized X-rays by NEXAFS-TXM," Nat. Photon **6**, 25–29 (2012).
[109]G. Polzonetti and C. Battocchio, "Functional and nanostructured materials investigated by XPS and NEXAFS spectroscopies," in *Advances in Macromolecules*, edited by M. V. Russo (Springer, Netherlands, 2010), pp. 165–217.
[110]J. Melke, A. Schoekel, D. Gerteisen, D. Dixon, F. Ettingshausen, C. Cremers, C. Roth, and D. E. Ramaker, "Electrooxidation of ethanol on Pt. An in situ and time-resolved XANES study," J. Phys. Chem. C **116**, 2838–2849 (2012).
[111]T. L. Reitz, P. L. Lee, K. F. Czaplewski, J. C. Lang, K. E. Popp, and H. H. Kung, "Time-resolved XANES investigation of CuO/ZnO in the oxidative methanol reforming reaction," J. Catal. **199**, 193–201 (2001).
[112]E. Vorobeva, S. L. Johnson, P. Beaud, C. J. Milne, M. Benfatto, and G. Ingold, "Local structural changes in excited Ti^{3+}:Al_{2}O_{3} studied by time-resolved XANES," Phys. Rev. B **80**, 134301–6 (2009).
[113]A. Lapini, P. Foggi, L. Bussotti, R. Righini, and A. Dei, "Relaxation dynamics in three polypyridyl iron(II)-based complexes probed by nanosecond and sub-picosecond transient absorption spectroscopy," Inorg. Chim. Acta **361**, 3937–3943 (2008).
[114]P. Gütlich and H. A. Goodwin, *Spin Crossover in Transition Metal Compounds I-III, Topics in Current Chemistry* (Springer, NewYork, 2004), pp. 233–235.
[115]V. Briois, P. Sainctavit, G. J. Long, and F. Grandjean, "Importance of photoelectron multiple scattering in the iron K-edge x-ray absorption spectra of spin-crossover complexes: Full multiple scattering calculations for several iron(II) trispyrazolylborate and trispyrazolylmethane complexes," Inorg. Chem. **40**, 912–918 (2001).

[116]W. Gawelda, V.-T. Pham, M. Benfatto, Y. Zaushitsyn, M. Kaiser, D. Grolimund, S. L. Johnson, R. Abela, A. Hauser, C. Bressler, and M. Chergui, "Structural determination of a short-lived excited iron(II) complex by picosecond x-ray absorption spectroscopy," Phys. Rev. Lett. **98**, 057401–4 (2007).
[117]M. Benfatto, A. Congiu-Castellano, A. Daniele, and S. Della Longa, "MXAN: A new software procedure to perform geometrical fitting of experimental XANES spectra," J. Synchrotron. Radiat. **8**, 267–269 (2001).
[118]B. O'Regan and M. Gratzel, "A low-cost, high-efficiency solar cell based on dye-sensitized colloidal TiO_2 films," Nature **353**, 737–740 (1991).
[119]M. K. Nazeeruddin, F. De Angelis, S. Fantacci, A. Selloni, G. Viscardi, P. Liska, S. Ito, B. Takeru, and M. Grätzel, "Combined experimental and DFT-TDDFT computational study of photoelectrochemical cell ruthenium sensitizers," J. Am. Chem. Soc. **127**, 16835–16847 (2005).
[120]P. Persson and M. J. Lundqvist, "Calculated structural and electronic interactions of the ruthenium dye N3 with a titanium dioxide nanocrystal," J. Phys. Chem. B **109**, 11918–11924 (2005).
[121]F. De Angelis, S. Fantacci, A. Selloni, M. K. Nazeeruddin, and M. Grätzel, "First-principles modeling of the adsorption geometry and electronic structure of Ru(II) dyes on extended TiO_2 substrates for dye-sensitized solar cell applications," J. Phys. Chem. C **114**, 6054–6061 (2010).
[122]X. Zhang, G. Smolentsev, J. Guo, K. Attenkofer, C. Kurtz, G. Jennings, J. V. Lockard, A. B. Stickrath, and L. X. Chen, "Visualizing interfacial charge transfer in ru-dye-sensitized TiO_2 nanoparticles using x-ray transient absorption spectroscopy," J. Phys. Chem. Lett. **2**, 628–632 (2011).